

Mainz Microtron MAMI**Collaboration:** A1**Spokesperson:** H. Merkel**Title:** Electric form factor of the neutron at $Q^2 = 1.5 \text{ (GeV/c)}^2$ using ^3He .

Authors: P. Achenbach¹, C. Ayerbe Gayoso¹, D. Baumann¹, J. Bernauer¹, R. Böhm¹, B. Boillat², D. Bosnar³, C. Carasco², M.O. Distler¹, L. Doria¹, J. Friedrich¹, W. Glöckle⁴, J. Golak⁴, P. Grabmayr⁵, W. Heil⁶, I. Jaegle², P. Jennewein¹, J. Jourdan², H. Kamada⁴, J. Krimmer⁶, B. Krusche², K.W. Krygier¹, M. Makek³, H. Merkel¹, T. Mertens², U. Müller¹, R. Neuhausen¹, A. Nogga⁴, L. Nungesser¹, A. Ott⁵, E.W. Otten⁶, J. Pochodzalla¹, M. Potokar⁷, D. Rohe², D. Rudersdorf⁶, S. Sánchez Majos¹, I. Sick², S. Sirca⁷, R. Skibiński⁴, G. Testa², R. Trojer², Th. Walcher¹, M. Weinriefer¹, H. Witała⁴, F. Zehr²

¹*Institut für Kernphysik, Universität Mainz*, ²*Institut für Physik, Universität Basel*, ³*Department of Physics, University of Zagreb, Croatia* ⁴*Institut für Theoretische Physik II, Ruhr-Universität Bochum*, *Institute of Physics, Jagiellonian University Cracow*, *Kyushu Institute of Technology, Kitakyushu*
⁵*Physikalisches Institut, Universität Tübingen*, ⁶*Institut für Physik, Universität Mainz* ⁷*Institut "Jožef Stefan", University of Ljubljana*

Contactperson: M.O. Distler, W. Heil and D. Rohe**Abstract of physics:** Measurement of the electric form factor of the neutron at $Q^2 = 1.5 \text{ (GeV/c)}^2$ using polarized ^3He as effective neutron target.**Abstract of equipment:** The experiment will employ the polarized ^3He -target developed at the University of Mainz. Spectrometer A will detect the scattered electron in coincidence with the recoiling particles in a scintillator array. The beam polarization will be measured with the Møller polarimeter.**MAMI-Specifications :**

beam energy: 1450 MeV
 beam current: min. $5.0 \mu\text{A}$ max. $20.0 \mu\text{A}$
 time structure: continuous beam
 polarization: yes

Experiment-Specifications :

hall: spectrometer hall
 beam line: standard to spectrometer hall
 spectrometer: particles: range of angles: out of plane:
 A e^- 78.6° -

special detectors: Segmented BC400 scintillator array with lead shielding.
 Central angle: 25.6°

targets and chamber : ^3He -cell with magnetic holding field and shielding box

Beam time request :

set-up without beam: 400 h
 set-up with beam: 30 h
 data taking: 390 h

Mainz Microtron MAMI

Collaboration A1: “Virtual Photons”

Spokesperson: H. Merkel

Proposal for an Experiment

**Electric form factor of the neutron
at $Q^2 = 1.5 \text{ (GeV/c)}^2$ using polarized ^3He**

Collaborators:

B. Boillat, C. Carasco, I. Jaegle, J. Jourdan, B. Krusche, T. Mertens, D. Rohe*,
I. Sick, G. Testa, R. Trojer, F. Zehr
(Institut für Physik, Universität Basel)

J. Golak, W. Glöckle, H. Kamada, A. Nogga, R. Skibiński, H. Witała
*(Institut für Theoretische Physik II, Ruhr-Universität Bochum;
Institute of Physics, Jagiellonian University Cracow; Kyushu Institute of Technol-
ogy, Kitakyushu)*

D. Bosnar, M. Makek
Department of Physics, University of Zagreb, Croatia

M. Potokar, S. Sirca
Institut "Jožef Stefan", University of Ljubljana

W. Heil*, J. Krimmer, E.W. Otten, D. Rudersdorf
(Institut für Physik, Universität Mainz)

P. Achenbach, C. Ayerbe Gayoso, D. Baumann, J. Bernauer, R. Böhm, M.O. Dis-
tler, L. Doria, J. Friedrich, P. Jennewein, K.W. Krygier, H. Merkel, U. Müller,
R. Neuhausen, L. Nungesser, J. Pochodzalla, S. Sánchez Majos, Th. Walcher, M. Wein-
riefer
(Institut für Kernphysik, Universität Mainz)

P. Grabmayr, A. Ott
(Physikalisches Institut, Universität Tübingen)

*Contact Person

1 Introduction

The electromagnetic form factors play an important role in our understanding of the structure of the nucleon. In particular the electric form factor G_{en} of the neutron is sensitive to its internal structure because it is not obscured by the total charge as in the proton. The neutron is a composite of gluons and (sea-)quarks which carry a fraction of charge. Measuring G_{en} at high Q^2 can be seen as investigating the neutron deep inside at a scale which becomes comparable to the size of (constituent) quarks. For example Q^2 of 1.5 (GeV/c)^2 corresponds to a spatial resolution of 0.2 fm. Accounting for the quantum features of the elementary particles and their strong interaction, QCD is the tool of choice to calculate the form factors. In the last years progress had been made with lattice and quenched lattice calculations but the available computer power still limits the results to pion masses of 0.5 GeV (or current quark masses 5 – 10 times higher than the physical value). Therefore sophisticated approximation methods have been used to extrapolate the results to the physical values. Recent attempts to reproduce the electromagnetic form factors of the proton and the neutron look promising [1].

Due to this limitation in QCD calculations a large variety of model-calculations with different assumptions had been developed. A few of them are shown in fig. 1 and will be mentioned here. In ref. [2] the relation of the first moments of the Generalized Parton Distribution (GPD) to the Dirac and Pauli form factor F_1 and F_2 are exploited. The latter can be expressed in terms of the Sachs form factors G_{en} and G_{mn} . Using a modified Regge ansatz all four form factors can be reasonably reproduced with only four free parameters.

Some authors are fitting all four form factors simultaneously using the vector meson dominance model. In this model the virtual photon couples to a vector meson rather than to the nucleon. In addition perturbative QCD is used to determine the behavior at large Q^2 . In fig. 1 the most recent dispersion-theoretical analysis of ref. [4] is shown. Contrary to ref. [3] this parameterization is not able to reproduce the strong fall-off in the recent $G_{\text{ep}}/G_{\text{mp}}$ data [5, 6]. The reason is that these data do not comply with the superconvergence relations from perturbative QCD.

The calculation of ref. [8] is based on the chiral soliton model while including explicitly vector mesons as dynamical degrees of freedom. In fig. 1 the B1-version of ref. [8] is shown, where the coupling constant of the ρ -meson is approximately fixed by the KSRF relation [7]. It is interesting to note that this model did predict the steep slope of the ratio $G_{\text{ep}}/G_{\text{mp}}$ long before it was measured [5, 6]. The magnetic and the charge radii of the nucleons are also well reproduced.

In ref. [9] light front dynamics is used to model the nucleon as a system of three relativistic quarks surrounded by a cloud of pions. The pionic cloud is important at low momentum transfer ($Q^2 < 0.3 \text{ (GeV/c)}^2$) whereas at high Q^2 the dynamic of the relativistic quarks play the dominant role. Independently from this work it was recognized in ref. [10] that a bump structure appears in all four form factors around Q^2 of $0.2 - 0.3 \text{ (GeV/c)}^2$. Using a phenomenological ansatz where the nucleon is modeled by a bare nucleon consisting of up and down quarks plus a polarization

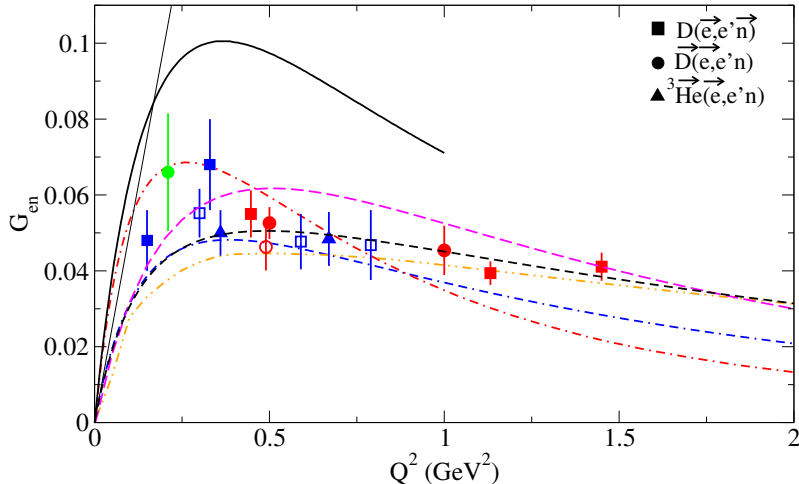


Figure 1: G_{en} extracted from quasi-elastic scattering of polarized electrons from D, $\bar{\text{D}}$ and ${}^3\text{He}$. The data are taken from refs. [16, 17, 18, 19, 20, 21, 22, 23, 24]. A selection of theories is shown: the quenched lattice calculation of ref. [1] (solid), the GPD based theory of ref. [2] (long-dashed), the light front dynamics of ref. [9] (dot-dot-dashed), the soliton model of ref. [8] (dot-dashed), the vector dominance models of ref. [3] (dot-dash-dashed) and ref. [4] (dashed). In addition the slope of G_{en} at $Q^2 = 0$ is drawn.

part, the bump was interpreted as resulting from the pion cloud. In the Breit frame this corresponds to a negative charge distribution reaching out as far as 2 fm. In contrast, the authors of ref. [11] separated the contribution of the two-pion continuum and found a peak at a distance of only 0.3 fm.

In the constituent quark model the pion cloud results from the repulsive force between pairs of d-quarks and the attraction between u- and d-quarks. From the classical point of view a picture of the neutron as a proton surrounded by a pion is suggested by the negative charge radius of the neutron r_n . This radius was measured via neutron transmission through Pb and Bi by [12, 13]. The charge radius is directly related to the neutron's rest frame internal charge distribution and is not dominated by the Foldy term. The latter is compensated by contributions from relativistic effects [14].

In ref. [15] an interesting relation was found between the ratio of the electric to magnetic form factor of the neutron to the multipole ratio C2/M1 of the $\text{N} \rightarrow \Delta$ transition using SU(6) flavor symmetry. Neglecting exchange currents C2 is only non-zero if the nucleon and/or the Δ contains d-waves, i.e if at least one of them is deformed. This is the only way to observe a possible quadrupole deformation because it can not directly measured for spin 1/2 particles. Recent measurements give a negative C2/M1 ratio over the range measured (up to $Q^2 = 4 \text{ (GeV/c)}^2$) which indicates a prolate deformation of the Δ . Within the error bars the relation to $G_{\text{en}}/G_{\text{mn}}$ was confirmed using experimental data. In particular this relation remains valid even when the SU(6) flavor symmetry is broken.

The electric form factor of the neutron is not only important to understand the

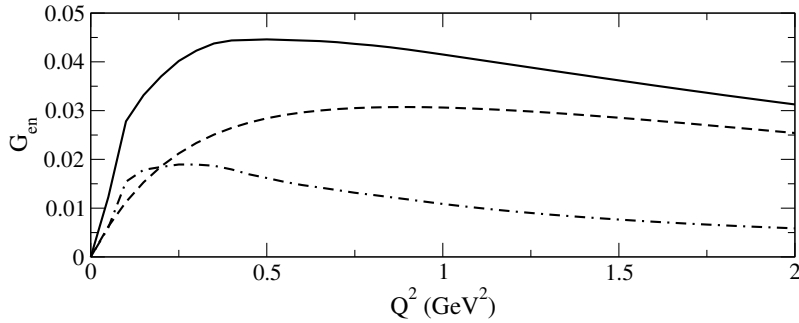


Figure 2: Separation of the result of ref. [9] (solid) into the contribution from the pion cloud (dot-dashed) and due to the relativistic movement of the quarks (dashed).

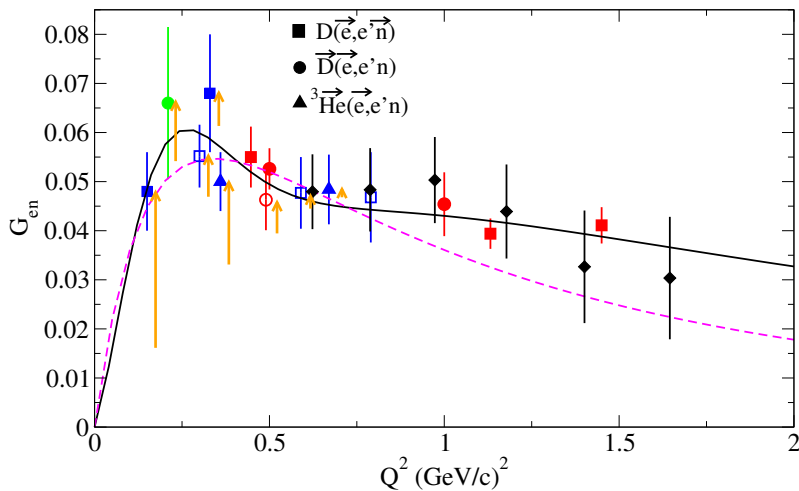


Figure 3: In addition to the data shown in fig. 1 the result from the analysis of [25] is shown. The dashed line represents the Galster fit [29] and the solid curve the result of [10]. For some of the experimental data points the correction due to the reaction mechanism beyond PWIA is indicated by arrows.

structure of the nucleon but also serves as ingredient in the analysis of processes involving electromagnetic interactions with complex nuclei. At high Q^2 the electric form factor of the proton and the neutron become comparable in size (at $Q^2 = 1.5 \text{ (GeV/c)}^2$ $G_{\text{en}} \approx 0.04$, $G_{\text{ep}} \approx 0.1$). Further G_{en} needs also to be known to determine the strangeness content in the nucleon. Here one measures an interference term between the electromagnetic and electroweak form factors.

2 Present data base and planned work

Electron scattering is a useful tool for probing the electromagnetic structure of the nucleon. Its coupling is weak compared to hadronic probes and therefore higher order diagrams with more than one-photon exchange are suppressed. However, such diagrams may become important as recently shown for the ratio $\mu_p G_{\text{ep}}/G_{\text{mp}}$.

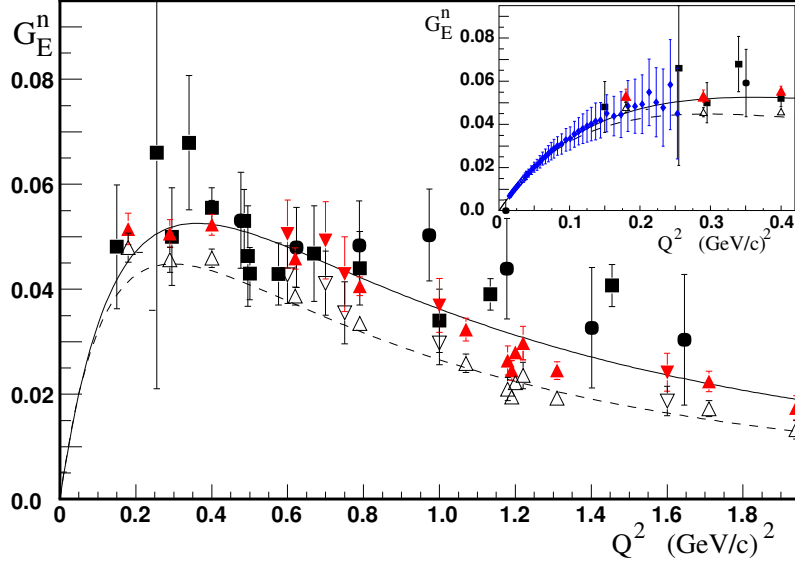


Figure 4: Same data as in fig. 3 with additional G_{en} -values extracted from F_π data [32, 33] using $\Lambda^2 = 0.71 \text{ GeV}^2$ (open triangles) and $\Lambda^2 = 0.86 \text{ GeV}^2$ (full triangles). In the insert additional pion data for the low Q^2 range are shown [34]. The figure slightly modified is taken from ref. [31].

Using the Rosenbluth separation leads to values close to one [26] whereas in the double-polarization experiment the form factor ratio drops steadily starting at Q^2 around 2 (GeV/c)^2 [5, 6]. Recent work revealed that the two-photon contribution, though only of the order of a few percent of the total cross section, amplifies in the Rosenbluth method due to the sensitive decomposition into the longitudinal and transverse part of the cross section. The results from the double-polarization method are barely affected.

G_{en} is particular difficult to measure due to its smallness which makes a Rosenbluth separation unpractical. The fact that pure neutron targets of sufficient density are not available, leads to the use of light nuclei like the deuteron and ^3He . Further it takes more effort to detect the neutron than the proton and the detection efficiency is much smaller. To circumvent this problem elastic e - d scattering was exploited to extract G_{en} from the deuteron structure function $A(Q^2)$ [29, 30] where the contribution from the deuteron magnetic form factor and therefore G_{mn} and G_{mp} are negligible. On the other hand the large contribution from G_{ep} has to be subtracted. Theoretical input is needed to remove contributions from the deuteron structure and to account for two-body currents (MEC's). Because the wave function of the proton in the deuteron has to be known the extraction of G_{en} depends on the model and the N-N potential. From such an analysis and using data up to $Q^2 = 0.8 \text{ (GeV/c)}^2$ with coarse statistical uncertainty the so called Galster fit was obtained [29], where the dipole form is modified in such a way that the slope at small Q^2 could be reproduced. The slope itself is related to the neutron charge radius ($\langle r_{en}^2 \rangle = -6dG_{en}(Q^2)/dQ^2$). The most recent result is drawn in fig. 1.

Originally the form of the Galster fit was chosen according to a modified dipole

form and therefore it is purely phenomenological. However, a theoretical justification was recently given in ref. [31]. It was shown that this parametrization can be derived from a model describing the nucleon as consisting of valence quarks and a pion cloud. The two parameters in the Galster form (extended version) are related to the pion electromagnetic form factor F_π and to the spectroscopic strength (= number) of the pions. Using this relation G_{en} can be extracted from F_π data and the neutron charge radius. The result is shown in fig. 4 for two values of Λ (dipole form factor $G_D = (1 + Q^2/\Lambda^2)^{-2}$). The larger value for Λ can be justified by the need of taking the core radius of the neutron instead of the extended charge distribution. Both fits shown as solid and dashed line are significantly lower than the G_{en} value at $Q^2 = 1.45 \text{ (GeV/c)}^2$ [22]. The rest of the G_{en} measurements are well described by the solid line. A similar behavior is observed for the original Galster fit (s. fig. 3).

A novel approach developed by ref. [25] exploits the quadrupole form factor $F_{C2}(Q^2)$ of the deuteron rather than a combination of monopole and quadrupole form factors which make up $A(Q^2)$. This is attractive as the contribution from two-body currents is relatively small and the sensitivity of G_{en} to the chosen N-N potential is significantly reduced compared to the analysis using $A(Q^2)$. Therefore this method allows to extract G_{en} with a smaller systematic error (s. fig. 3). However, at low Q^2 the statistical error of F_{C2} is large because the monopole form factor F_{C0} dominates the T_{20} data and the sensitivity to F_{C2} is reduced. Thus, the analysis using $A(Q^2)$ becomes superior for $Q^2 < 0.4 \text{ (GeV/c)}^2$.

Double-polarization experiments in exclusive reactions are a sensitive tool to measure G_{en} . Here the longitudinally polarized electron beam scatters quasielastically on deuterons or ^3He , which is either polarized itself or the polarization of the knock-out neutron is detected [35]. The asymmetry with respect to the electron helicity contains then an interference term $G_{\text{en}} G_{\text{mn}}$ which amplifies G_{en} by G_{mn} . The sensitivity to G_{en} is largest in the perpendicular asymmetry A_\perp , where the spin direction of the target spin is perpendicular to the momentum transfer (or the polarization of the scattered neutron is perpendicular to its momentum, respectively). In contrast the parallel asymmetry A_\parallel does not depend on form factors (for G_{en} small) and therefore can serve for calibration or normalization.

The data points for G_{en} shown in fig. 1 as a function of Q^2 were all derived from double-polarization experiments in quasielastic kinematics using both methods, target and recoil polarization. The scattered electron and the knocked-out neutron are detected in coincidence to avoid the contribution from the reaction (e,e'p). As targets deuterium and ^3He were used. Each method and target has its own advantages and problems. The recoil method using unpolarized D-target suffers from the low detection efficiency in a neutron polarimeter but can profit from the high-dense and pure D. Polarized deuterium requires a very high magnetic field (several Tesla) which bends the trajectories of the charge particles in the vicinity of the target. Further the dense \vec{D} is only available as a composite (e.g. ND_3) which leads to dilution of the neutron polarization. $^3\vec{\text{He}}$ has an interesting spin structure which allows its application as effective polarized neutron target, but the target density is low compared to a liquid deuterium target.

The highest Q^2 so far, at which G_{en} was measured is 1.45 (GeV/c)^2 . It was

determined at Jefferson Lab in hall C using an unpolarized deuterium target and a neutron polarimeter. Using the same method and a similar setup it is planned by the same group to measure G_{en} at $Q^2 = 4.3 \text{ (GeV/c)}^2$ with a total uncertainty of 0.002 [36].

Another experiment E02-013 is scheduled for 2006 to measure G_{en} at $Q^2 = 1.3, 2.4$ and 3.4 (GeV/c)^2 with expected statistical errors for $\Delta G_{\text{en}}/G_{\text{en}}$ of 8.7 %, 14.2 % and 13.8 %, respectively. The systematic uncertainty is estimated to 10 % independent of Q^2 . This experiment will use polarized $^3\vec{\text{He}}$ as the present proposal. In sec. 4 the proposed experiment and E02-013 will be compared. It will be shown that the systematic error can be significantly reduced using the method suggested for the present proposal.

3 Proposed experiment

We propose to measure G_{en} at a central momentum $Q^2 = 1.5 \text{ (GeV/c)}^2$ using the semi-exclusive reaction $^3\vec{\text{He}}(\vec{e}, e'n)$ in quasielastic kinematics. The scattered electrons will be detected in spectrometer A which is part of the three-spectrometer-facility at MAMI. The Cerenkov detector installed in the spectrometer provides a clean pion rejection. The knocked-out neutron is detected in a scintillator array. Protons will be recorded as well and distinguished from neutrons according to their different energy deposition in two thin scintillators which serve as veto detectors (ΔE). The details of the setup will be described in sec. 3.2. Experience with such a setup exists from the G_{en} measurements in 1997 and 2000 at $Q^2 = 0.67 \text{ (GeV/c)}^2$ [39, 21] as well as from the experiment "The structure of ^3He " in 2003 [37][38]. To increase the neutron detection efficiency for the proposed experiment it is planned to double the thickness of the scintillator material. The performance of the $^3\vec{\text{He}}$ target is improving and further developments are in progress.

Q^2 (GeV/c ²)	q GeV/c	E GeV	E' GeV	θ_e deg	θ_q deg
1.50	1.47	1.45	0.647	78.6	25.6

Table 1: Central kinematics.

The kinematics of the proposed experiment is shown in Table 1. Such a high momentum transfer becomes measurable at MAMI with the extension to a maximum available electron energy of 1.5 GeV. This is realized with a Harmonic Double Sided Microtron (HDSM) where the electrons will circulate another 43 times after having passed the existing microtron MAMI B. Beam in MAMI C is expected at the end of 2005 or beginning of 2006.

3.1 Method to extract G_{en}

The experimental method to determine G_{en} relies on measuring the electron-target asymmetry. This has the advantage that no absolute cross section measurements are needed which avoids the effort (and systematic errors) of determining absolute efficiencies, solid angle and luminosity. The experimental electron-target asymmetry is obtained via

$$A_{\text{exp}} = \frac{N^+/L^+ - N^-/L^-}{N^+/L^+ + N^-/L^-}, \quad (1)$$

with L^+ (L^-) are the integrated charge and N^+ (N^-) the number of events for positive (negative) electron helicity. The electron helicity is flipped every second randomly. A valid event requires an electron in the spectrometer and a neutron in the scintillator within the coincidence timing window. Accidentals appearing as background outside the coincidence time peak are subtracted and its asymmetry will be checked. The background is usually unpolarized and can be taken into account by a dilution factor V .

In general the asymmetry A can be decomposed according to the direction of the target spin which is given by the angles θ_S and ϕ_S with respect to the momentum transfer \vec{q} and the scattering plane.

$$A = A_{\perp} \sin \theta_S \cos \phi_S + A_{\parallel} \cos \theta_S \quad (2)$$

A_{exp} is related to the asymmetry calculated from theory A_{theo} by

$$A_{\text{exp}} = P_e P_n V A_{\text{theo}}. \quad (3)$$

P_e and P_n are the polarization of the electron beam and the neutron, respectively. Depending on the experimental conditions further dilution factors have to be taken into account (s. below). A_{theo} contains the electromagnetic form factors but also depends on the reaction mechanism involved. For scattering on a free neutron one has

$$A_{\perp} = \frac{2\sqrt{\tau(1+\tau)} \tan(\theta/2) G_{\text{en}} G_{\text{mn}}}{G_{\text{en}}^2 + G_{\text{mn}}^2 (\tau + 2\tau(1+\tau) \tan(\theta/2))} \quad (4)$$

$$A_{\parallel} = 2 \frac{\tau \sqrt{1+\tau + (1+\tau)^2 \tan^2(\theta/2)} \tan(\theta/2) G_{\text{mn}}^2}{G_{\text{en}}^2 + G_{\text{mn}}^2 (\tau + 2\tau(1+\tau) \tan(\theta/2))}. \quad (5)$$

Due to its special nuclear structure polarized ${}^3\vec{\text{H}}\text{e}$ serves in good approximation as a polarized neutron target in quasielastic kinematics. The spin of ${}^3\vec{\text{H}}\text{e}$ is mainly carried by the neutron whereas the two protons reside in a S-state and their spins cancel each other. This part of the wave function dominates for moderate missing momentum p_m of 150 MeV/c and less. For large $p_m > 200$ MeV/c the D-wave contribution takes over and the polarization of the neutron in ${}^3\vec{\text{H}}\text{e}$ drops whereas the protons get polarized. This interplay of the ${}^3\text{He}$ wave function is best visualized by fig. 5 which is based on a Faddeev calculation of Schulze and Sauer [40, 41]. Here the spin-dependent momentum distribution for the neutron and the proton bound in ${}^3\vec{\text{H}}\text{e}$ is shown. In the proposed experiment more than 80 % of the count rate is due to neutrons with $p_m < 150$ MeV/c.

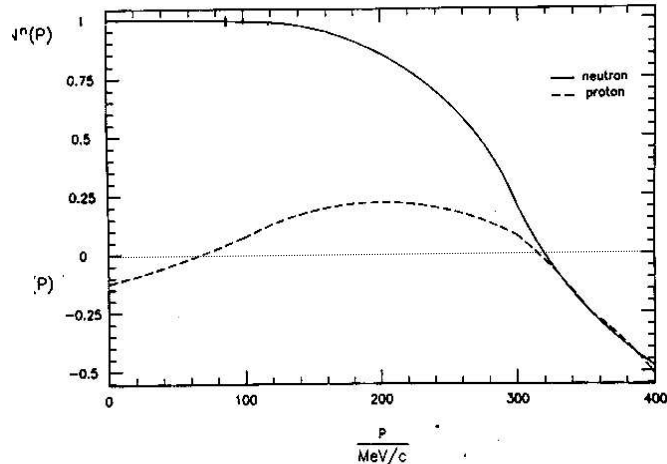


Figure 5: Spin dependent momentum distribution for the neutron and the proton in ${}^3\vec{\text{He}}$. The figure is taken from [40].

The asymmetries in the reactions ${}^3\vec{\text{He}}(\vec{e}, e'p)$ and ${}^3\vec{\text{He}}(\vec{e}, e'n)$ for large p_m up to 250 MeV/c were measured at $Q^2 = 0.3$ (GeV/c) 2 in 2003 and are under analysis. These data are sensitive to the D-state of the ${}^3\text{He}$ wave function (s. Proposal "The structure of ${}^3\text{He}$ "). The results for the asymmetries in the two- and three- body breakup in ${}^3\vec{\text{He}}(\vec{e}, e'p)$ are published and in good agreement with the theory of Golak [38].

G_{en} is determined from the ratio of the asymmetries A_{\perp} and A_{\parallel}

$$\frac{A_{\perp}}{A_{\parallel}} \propto \frac{G_{\text{en}}}{G_{\text{mn}}} \quad (6)$$

instead of A_{\perp} alone. This has several advantages:

- The polarization product $P_e P_n$ drops out. Therefore the systematic error introduced with the two measurements of absolute polarizations can be considerably reduced. Only fluctuations of the polarization have to be taken into account which requires knowledge of it on a relative scale only and can be much more accurately determined.
- An important point is that one can only measure the target polarization P_T but not the intrinsic polarization P_n of the neutron which is lower than P_T and depends on the momentum of the neutron in ${}^3\text{He}$ (s. fig. 5). The correction factor accounting for the reduction in the intrinsic neutron polarization has to be provided by theory. In the ratio of eq. 6 it drops out.
- The dilution factor V due to unpolarized background cancels.
- Another dilution of the asymmetry comes from charge conversion of protons into neutrons in the lead wall (2 cm) in front of the neutron detector (s.

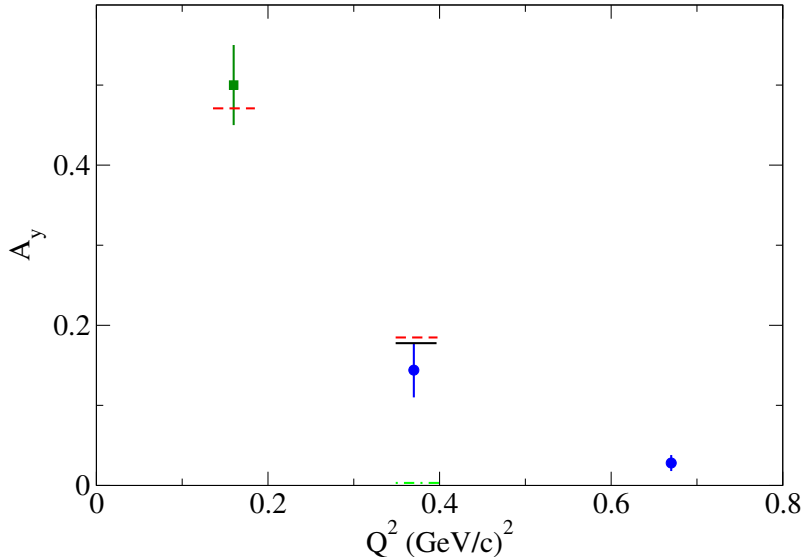


Figure 6: Results for the target analyzing power A_y measured at NIKHEF (square) and MAMI (circles) compared to Faddeev calculations treating FSI and MEC (solid), FSI only (dashed) and neglecting charge exchange (dot-dashed).

sec. 3.2.2). It increases with the thickness of the lead. Experimentally the conversion factor can be determined using a hydrogen target but detecting neutrons in the scintillator ($H(e,e'p)+Pb(p,n)$). From a former measurement at $Q^2 = 0.67$ (GeV/c)² [42, 21] the dilution from this effect is expected to be ≈ 10 %. This value is already corrected for the different cross section ratio for protons and neutrons at $Q^2 = 1.5$ (GeV/c)². In sec. 3.2.2 it will be compared to simulations performed with Geant4. Neglecting the small polarization of the protons in the covered missing momentum range this dilution factor will also drop out in the asymmetry ratio of eq. 6.

To extract G_{en} using eq. 6 the magnetic form factor G_{mn} has to be known. It was recently measured in Hall B [43, 44] up to $Q^2 = 4.8$ (GeV/c)². At 1.5 (GeV/c)² a statistical error bar of 0.6 % and a systematical uncertainty of 1.4 % is expected. Therefore we will assume an uncertainty of 2 % for G_{mn} .

Eqs. 4 and 5 are only valid for a free neutron. FSI and MEC will lead to modifications of the asymmetry and therefore corrections to G_{en} have to be provided by the theory. Currently the three-body system, ${}^3\text{He}$, is solved using the non-relativistic Faddeev equation treating MEC and FSI on an equal footing [45]. A measurement sensitive to FSI and MEC effects is the target analyzing power A_y which can be determined by using an unpolarized electron beam with target spin incident to the scattering plane. In the past it was measured for three different Q^2 at NIKHEF [46] and MAMI [21] (fig. 6). From this measurement one can expect that contributions beyond PWIA become negligible at high Q^2 . Whereas the corrections at small Q^2 are ≈ 50 % or even larger they drop to ≈ 3 % at $Q^2 = 0.67$ (GeV/c)² [21]. It is interesting to note that the main distortion in the reaction ${}^3\vec{\text{He}}(\vec{e}, e'n)$ results from charge-exchange between the proton and the neutron. The

cross section for charge-exchange is known to decrease with increasing Q^2 . From fig. 6 it is also obvious that MEC contributions are small if one compares the calculations with and without MEC included. MEC's become important in the wings of the quasielastic peak, i.e. at high missing momentum, but are negligible at the top of the quasielastic peak for $Q^2 \gtrsim 0.3$ (GeV/c)². At low $Q^2 \lesssim 0.2$ (GeV/c)² the effect from MEC becomes sizable already on top of the quasielastic peak. In addition MEC contributions decrease with increasing Q^2 . At large Q^2 (> 1 (GeV/c)²) the MEC amplitude drops relative to the PWIA amplitude with a factor $(1+Q^2/\Lambda^2)^{-2}$ with $\Lambda = 0.8 - 1$ (GeV/c)² [47]. In fig. 3 the size of the theoretical correction applied to G_{en} is indicated by arrows. For the moment we will assume an uncertainty due to a nuclear correction of 3 %.

At the moment there are no exact calculations available for ³He which can treat MEC and FSI at high Q^2 . Both, the Faddeev calculation of ref. [48] and the S-matrix formalism of ref. [49] are non-relativistic and valid only below the pion-threshold. The c.m. energy available in the 3N-system E_{3N} is calculated for the 3-body breakup via

$$E_{3N} = \sqrt{(M_{He} + \omega)^2 - |\vec{q}|^2} - 2M_p - M_n \quad (7)$$

For the quasielastic kinematics given in Tab. 1 this leads to $E_{3N} \approx 460$ MeV which is certainly above the pion threshold and would even allow to excite the Δ resonance. This is avoided by the use of kinematical cuts and by the limited momentum acceptance of the electron spectrometer. Therefore it is justified to apply the existing Faddeev formalism but accounting for relativistic effects. This was done for a similar setup at $Q^2 = 0.67$ (GeV/c)² where the reaction ³He($\vec{e}, e'p$) was examined and compared with a theoretical approach including only the rescattering term of the spectators but treating the kinematics and the current operator relativistically. Good agreement between data and theory was achieved [50]. It also became clear that the use of the relativistic current operator is less relevant whereas the relativistic treatment of the kinematics is important.

Such a calculation was performed by J. Golak for the kinematics of this proposal. In addition to the central electron kinematics the electron scattering angle was varied by $\pm 4^\circ$. These three electron kinematics were combined with five angles for the knocked-out neutron equally spaced over the acceptance of the hadron detector in the scattering plane. This provides a coarse grid over the acceptance of the setup for the proposed G_{en} measurement which is sufficient for an estimation of deviations from PWIA. In particular it covers also the wings of the quasielastic peak where FSI contributions might be enhanced. The calculation was performed with the rescattering included and in PWIA for comparison. The underlying force is the CD Bonn potential. The kinematics as well as the 1-body current operator are always treated relativistically. Two versions for the ³He ground state wave function Ψ_b and the nucleon-nucleon t -matrix acting within the 2 – 3 pair (rescattering) are used. One version treats Ψ_b and the t -matrix relativistically ("boosted", solid lines in the following figures), in the other calculation both quantities are taken non-relativistically (dashed lines). For the first case a relativistic potential had to be derived which gives the same N-N phase shifts as the non-relativistical potential when used with the relativistic Lippmann-Schwinger equation [54]. The Coulomb

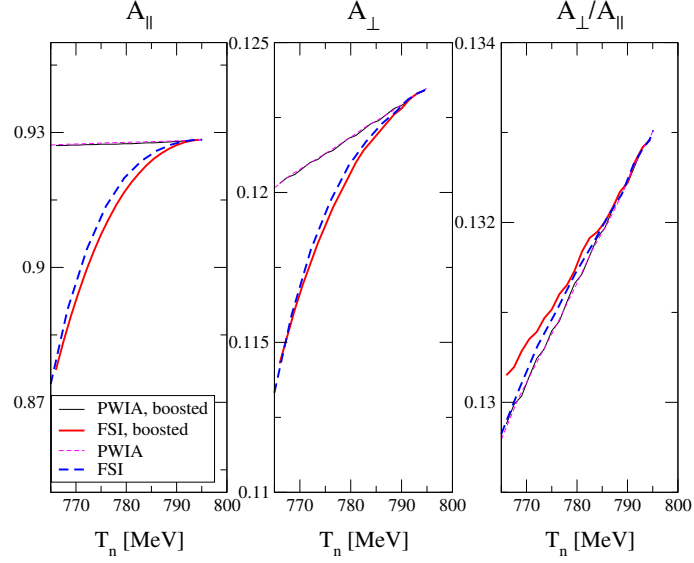


Figure 7: Relativistic calculation of J . Golak as a function of the kinetic energy of the outgoing neutron for the central kinematics in Tab. 1. A_{\parallel} , A_{\perp} and its ratio is plotted for PWIA, FSI (rescattering part) and the two versions indicated in the text.

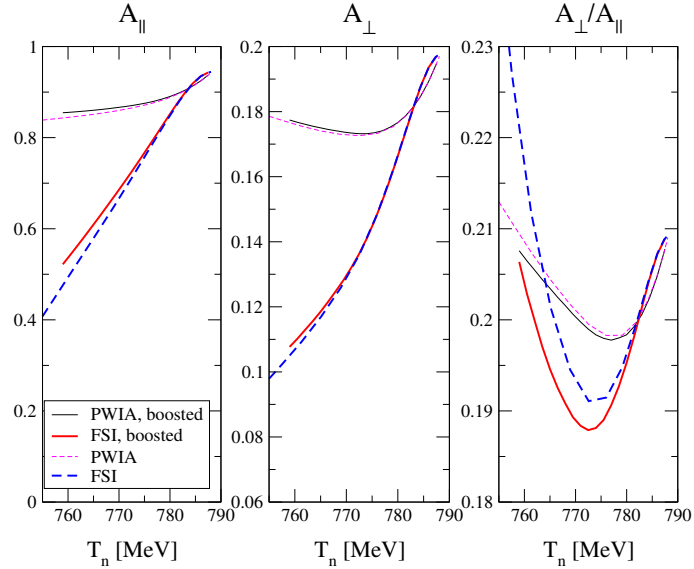


Figure 8: Same as fig. 7 but using a neutron angle of 19.3° .

force in the 2 – 3 pair is neglected. As can be seen from figs. 7 and 8 the difference in the resulting asymmetry between the two versions is small. The same is true for the cross section. An interesting feature of the cross section is that it drops with decreasing kinetic energy of the neutron T_n and becomes even steeper once FSI is included. 5 MeV below the maximum value possible for T_n the cross section has decreased already by an order of magnitude. This helps to suppress effects from FSI because the deviation of the asymmetry from PWIA gets larger with decreasing

T_n which corresponds to increasing E_m and p_m . In fig. 7 the asymmetries A_\perp , A_\parallel and their ratio, proportional to G_{en} , are plotted as function of T_n for the central kinematics. Compared to PWIA the asymmetries decrease much faster with T_n but both asymmetries, A_\parallel and A_\perp seem to decrease in the same way. This keeps the ratio A_\perp/A_\parallel close to the value for PWIA even for large T_n . At smaller neutron angle, i.e. in the wing of the quasielastic peak, the effect of rescattering is larger as shown in fig. 8 but still small. In particular the asymmetry ratio stays close to the PWIA value for the first 10 MeV below the maximum. Compared to the top of the quasielastic peak the cross section yields three orders of magnitudes smaller. Using the 15 kinematics to average over the acceptance of the setup there is only a negligible difference between the asymmetries obtained in PWIA and with FSI included.

Up to now there are no full 3N-calculations including relativity available. An important step toward it is the development of a Lorentz boosted NN potential. In ref. [54] such a potential was obtained and used in a relativistic 3N-Faddeev equation for the bound state to calculate the triton binding energy. It is hoped that the feasibility of measurements at high Q^2 now available at two facilities, Jlab and MAMI, using polarized ${}^3\vec{\text{H}}\text{e}$ will strengthen the effort of the theoriest to extend their theory to these Q^2 region, including the treatment of full FSI and MEC. This might be a similar situation as in the late 80'ies where a G_{en} measurement was proposed at $Q^2 = 0.35 \text{ (GeV/c)}^2$ [51] and where only a limited knowledge about the effects of FSI at this Q^2 was available [52, 53].

3.2 Experimental setup

The experimental realization is similar to the setup for the G_{en} measurement at $Q^2 = 0.67 \text{ (GeV/c)}^2$ performed in 1997 and 2000 at the three-spectrometer facility at MAMI. In the meantime the performance of the target has been significantly improved (s. sec. 3.2.1). The experiment performed in 2003 to examine the structure of the ${}^3\vec{\text{H}}\text{e}$ took already advantage of it. For this experiment a second scintillator array, constructed in the same way as the old one, was used to measure nucleons at the same time left and right of the quasielastic peak. To increase the neutron detector efficiency in the proposed experiment the two detectors will be combined to one (s. fig. 9).

3.2.1 Polarized beam and target

Since several years polarized electrons are produced from a strained GaAsP cathode which nowadays reach currents up to $80 \mu\text{A}$ and polarizations P_e of 75 to 80 %. The electron current is measured continuously and helicity dependent with a Faraday cup which allows to correct the measured asymmetry by the luminosity (s. eq. 1). The electron polarization is determined with a Møller polarimeter [55] located several meters upstream of the target pivot in the experimental hall. Within a few minutes P_e is measured with a statistical error of better than 2 %. The systematic uncertainty is smaller than 2 %. The total time needed for a Møller measurement

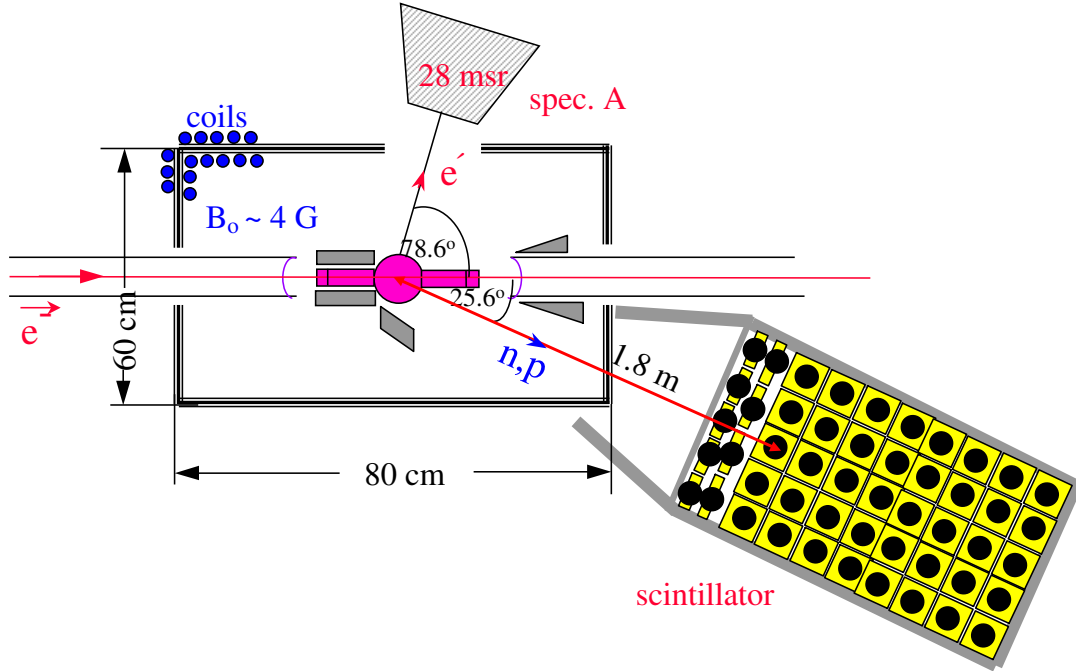


Figure 9: Experimental setup for the G_{en} measurement at $Q^2 = 1.5 \text{ (GeV/c)}^2$.

is approximately 15 minutes, during which production data taking is stopped. It is planned to measure the polarization twice a day just before changing the target cell. This procedure was utilized during the experiment in 2003.

In front of the target ($\approx 1 \text{ m}$) a beam spot monitor will be installed to ensure that the electron beam passes the 1 cm wide target windows without damaging the target. It consists of a ZnS screen which is remotely controlled by the MAMI personal and used for alignment of the electron beam. The vacuum beam line upstream and downstream is closed with $20 \mu\text{m}$ thick Be-foils. To avoid damage of the Be-foils caused by ozone produced by ionization of oxygen due to the electron beam a N_2 flow is installed.

The ^3He target is kept polarized in a homogeneous magnetic field of 4 Gauss. Its direction and consequently the direction of the ^3He spins can be rotated in three dimensions by three independent coils wrapped around a rectangular box. The direction of the magnetic field is measured with a precision of $< 0.2^\circ$ using a fluxgate magnetometer placed close to the target. The box is made out of 2 mm thick μ metal and iron plates to shield the magnetic stray field from the spectrometer. Towards the spectrometer a hole is cut into the box to let the electrons pass.

The container for the polarized ^3He consists of a sphere ($\text{O} 9 \text{ cm}$) with cylindrical extensions attached. It is made out of quartz glass and two thin Be-foils ($50 \mu\text{m}$) as entrance and exit window for the electron beam. In total the target cell is 25 cm long. This allows to suppress background from the target windows due to lead blocs placed close to the target.

The ^3He gas is polarized via metastable optical pumping which requires pressures

of 1 mbar to be feasible. The first excited metastable state (2^3S_1) is reached via gas discharge, from which the polarization of photons to the atomic electrons is transferred by resonant absorption of circularly polarized light. Nuclear polarization is obtained by collisions between unpolarized atoms in the ground state and polarized atoms in the 2^3S_1 . To reach high pressures the gas is subsequently compressed in a non-magnetic piston and 5 bar ^3He is filled into the target cell. With the upgraded ^3He polarizer and compressor the transfer of the ^3He gas from the low pressure optical pumping cells to the high pressure target cell is performed without polarization losses. Therefore a target polarization P_T of 70 % is reached at a reduced flow of 2 bar liter per hour [56]. This requires about one hour to fill the target cell.

The target cell is then transported to the three-spectrometer hall and put in place into the target box. The average polarization obtained depends on the starting polarization $P_{T,o}$, the total relaxation time T_1 and the duration τ of exposure to the beam ($\overline{P_T} = 1/\tau \int_0^\tau P_{T,0} \exp(-t/T_1) dt$). The total relaxation time results from different processes. The wall relaxation, i.e. the loss of polarization due to collisions of ^3He atoms with the wall of the target container (more precise interaction with para- and ferromagnetic centers), is reduced by cesium coating and an appropriate degaussing procedure. At ≈ 1 bar relaxation times of more than 100 h are routinely achieved in quartz cells. At higher pressure the dipole-dipole coupling between the ^3He atoms limits the storage time ($T_{1,dipol} = 800/p[\text{bar}]$ [57]). The contribution caused by inhomogeneities in the magnetic field is negligible at $\Delta B/B = 5 \cdot 10^{-4}$ achieved in the box over the region of the target cell. A non-negligible loss of polarization comes from ionization of ^3He atoms by the electron beam. Ionized ^3He atoms can form loosely bound $^3\text{He}_2^+$ molecules and the nuclear spin polarization is transferred to rotational angular momentum. With the additive of N_2 in the order of 10^{-3} the number of $^3\text{He}_2^+$ molecules drastically is reduced (quenched) and thus the relaxation time increases from minutes to $T_{1,beam} = 150 - 200$ h at $10 \mu\text{A}$ [42, 58]. In the experiments performed with ^3He at MAMI the beam current was limited to $10 \mu\text{A}$ which was partly due to high rates (in "The structure of ^3He ") or due to the performance of the polarized electron source in former times. However, the performance of the experiment is given by the figure of merit (f.o.m.) which is proportional to the averaged polarization $\overline{P_T}^2$ times the beam current. The f.o.m. in fig. 10 was calculated for a target cell filled with 5 bar ^3He and $T_{1,wall} = 75$ h (measured at a pressure of 2 bar on target cells prepared for the experiment in 2003). The dipole relaxation time was taken into account. As example two values for $T_{1,beam}$, 1500 h and 2000 h per μA , were chosen. As expected the change of the target twice a day increases the f.o.m. considerably compared to once a day. Changing the target cell takes about 1 hour. This mode was also chosen in former experiments. More important, the f.o.m. steadily increases with increasing beam current, even if the averaged polarization $\overline{P_T}$ decreases due to the shortened total relaxation time caused by $T_{1,beam}$. In the last experiment 2003 an averaged polarization of 50 % was achieved and relaxation times under electron beam conditions of up to 45 h. This T_1 agrees with the one obtained accounting for all the contributions mentioned above. However, it was observed that T_1 was only about 25 - 30 h for target cells used the first time under beam condition and then continuously increased with each refill.

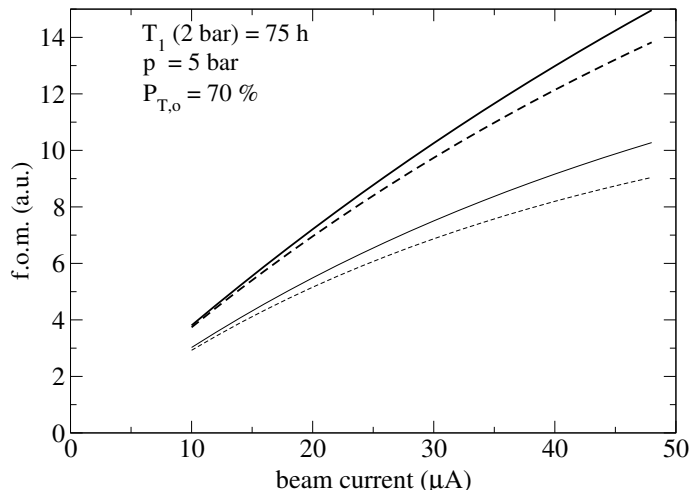


Figure 10: The figure of merit calculated as P_T^2 times the beam current for two different exchange times of the target, 12 h (thick lines) and 24 h (thin lines), and two partial relaxation times of 1500 h (dashed) and 2000 h (solid) per μA .

This process is not entirely understood. It is speculated that it might be caused by outgassing of the glue used to attach the copper windows. This outgassing could be initiated by electron collisions. Therefore the average polarization achieved in 2003 was only 50 %. In principle with $P_{T,o} = 70\%$ in the beginning one could reach an average polarization of 61 % under optimal conditions. Since this value was never reached yet an average polarization of 50 % will be assumed for the beam time estimate.

The target polarization is monitored by AFP (Adiabatic Fast Passage) and NMR (Nuclear Magnetic Resonance) techniques. During the AFP measurement the direction of the spin is reversed and the change in the magnetization is measured by a magnetometer. Only a fraction (0.1 - 0.2 %) of the polarization is destroyed per AFP shot. With this method the polarization is determined with a relative systematic error of 4 %. It was compared to and found to be in agreement with an absolute polarization measurement performed at the TRIGA reactor of the Mainz University [59]. This method exploits the polarization-dependence of the neutron-flux through the ^3He -container. Due to the reversal of the spin during AFP the data acquisition has to be stopped. Therefore this measurement is performed every 4 hours only whereas the NMR technique is used every 10 minutes. With NMR only the relative polarization can be measured. It serves to determine T_1 and as online control for the polarization.

3.2.2 Neutron detector

The two scintillator arrays were already used in the experiment "The structure of ^3He " as stand-alone hadron detectors to identify neutrons and protons. With the modifications described below they can be combined to one large neutron detector as shown in fig. 9.

The two scintillator arrays have identical design. Each detector consists of four layers of five BC400 scintillator bars of the size $50 \times 10 \times 10 \text{ cm}^3$. The front layer with the active size of $50 \times 50 \text{ cm}^2$ will be placed 180 cm from the reaction vertex. This results in a solid angle of 77 msr which is reduced for the subsequent layers. Due to its segmentation the resolution in the scattering plane is about 0.9° for the front layer. This assumes a rectangular distribution over the width of the scintillator bar. The out-of-plane angle can be reconstructed using the difference of the TDC signals from the two photomultipliers which are mounted on either side of the scintillator bar. In a similar setup a resolution of 0.8° [50] was achieved. To discriminate between protons and neutrons two layers of thinner scintillator bars are attached to the front which serve as veto detectors (ΔE 's). In the previous experiment low energy nucleons ($\approx 150 \text{ MeV}$) were detected and this required thin ΔE of 2 mm. In the present proposal the nucleons have kinetic energies in the range of 730 to 840 MeV and thus, as nearly minimizing ionizing particles, deposit less energy. The high energy protons will lose $\approx 2.7 \text{ MeV}$ ($> 2 \text{ MeV}$) per centimeter scintillator material. Therefore the ΔE 's will be replaced by 1 cm thick ones which were already used for the G_{en} measurement at $Q^2 = 0.67 \text{ (GeV/c)}^2$. For comparison, the 350 MeV protons at this kinematics deposited 3.5 MeV/cm.

As shown in fig. 9 the whole detector consists of eight layers of scintillator bars. Different detector configurations were tried out with the aim to optimize the neutron detector efficiency with the existing material. These studies using Geant4 are described in sec. 3.2.3. The neutron detector will be surrounded by 10 cm thick lead walls against electromagnetic background. In addition, 10 cm thick lead plates in a conical arrangement ("snout") will be placed between the target box and the detector. The front window facing the target will be covered by 2 cm lead. In a similar setup G_{en} at $Q^2 = 0.67 \text{ (GeV/c)}^2$ was measured at $\theta_q = 32^\circ$. The contribution from accidentals was not prohibitive for the measurement using the electronic scheme described below. In the e-n coincidence time spectrum with the spectrometer the background was 4 % when neutrons were selected in the scintillator. For protons it is even smaller. In case of an unexpected high single rate the lead thickness can be even increased because the nucleons at 800 MeV will still pass. The misidentification of protons as neutrons due to conversion in the lead will be measured using a target cell filled with hydrogen instead of ^3He . Furthermore, the dilution factor drops out to first order in the ratio of the perpendicular and parallel asymmetry. The optimal thickness will be found during the test beam time.

The lead shielding used for the two stand-alone detectors was vertically segmented in five pieces plus the top and the bottom plate. For the new arrangement as shown in fig. 9 a new lead housing would be needed. However, if one would omit the last layer and use a tight new stand for bars and veto detectors, it would fit into the old lead housing (clearance in depth: 850 mm). This less costly solution is considered in sec. 3.2.3 with respect to the achievable neutron efficiency.

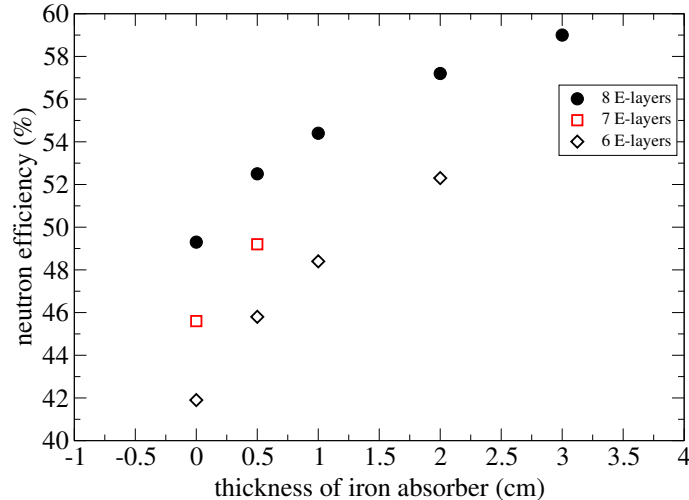


Figure 11: Neutron efficiency for 6, 7 and 8 E-bar layers as a function of the thickness of the iron absorber between the E-bars.

3.2.3 Neutron detector efficiency

The simulation package Geant4 is a toolkit for the passage of particles through matter [60]. It was used to examine several configurations for the scintillator array to achieve the largest neutron efficiency ϵ_n with the existing scintillator material. These configurations were compared to an array of reduced size which would fit into the existing lead shielding box. Then the total thickness of the array would be limited to 85 cm. The two layers of ΔE and the cross beams of the stand need 15 cm.

In the simulation the energy of the neutrons were equally distributed between the lowest and highest energy accepted by the detector setup shown in fig. 9. For the kinematics in Tab. 1 this corresponds to 0.73 GeV and 0.84 GeV. In addition, the angle of the flight path of the particle relative to the detector was varied to illuminate the first active layer of the detector uniformly. This accounts for the reduced solid angle of the subsequent layers. The simplified angular distribution overestimates slightly the effect and will lead to smaller neutron efficiencies. Common to all detector configurations studied is the 10 cm thick lead surrounding and the two layers of ΔE 's. The number of E-bar layers which consists of five scintillator bars each, were varied. Optionally absorber plates out of iron were put in between the E-layers and ϵ_n was studied as a function of the thickness of the iron. An additional absorber increases ϵ_n due to the increased probability to produce charged particles which deposit energy in the subsequent E-layer. The amount of energy deposited in each E-bar and ΔE was stored in a ROOT file. Then cuts on the deposited energy in the ΔE 's and E-bars were applied. To identify a particle as a neutron it was required that the energy loss in each ΔE is less than 1.5 MeV. Charged particles at this kinematics loose at least 2 MeV in a 1 cm thick ΔE .

First the simulation was checked using a detector setup used in 2003 to measure G_{en} at $Q^2 = 0.25 \text{ (GeV/c)}^2$. Neutrons of energies 0.089 to 0.175 GeV were identified

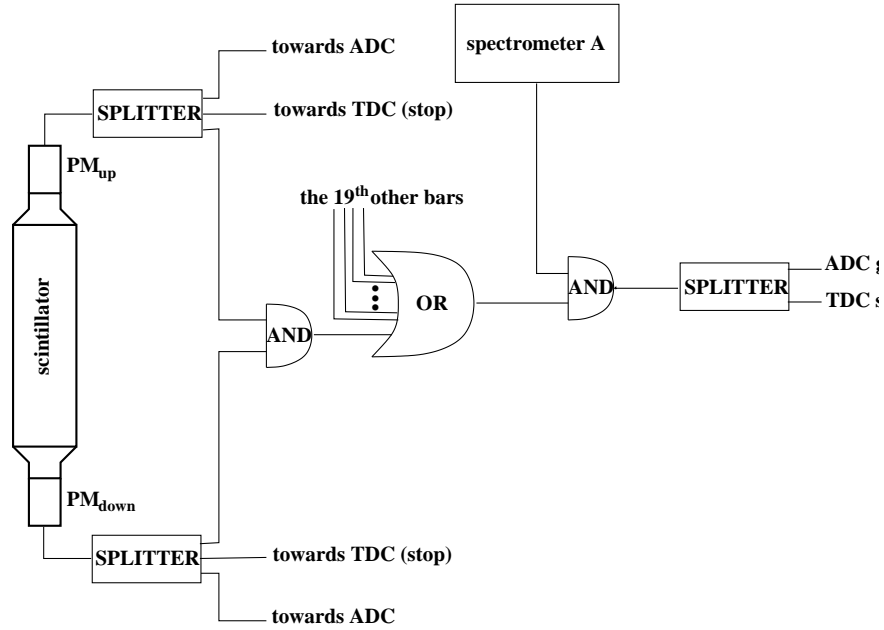
in 2 mm thick ΔE 's after transversing a 2 mm lead shielding. The threshold in the E-bars was 18-20 MeV. The neutron efficiency was obtained from the detected number of neutrons to protons scaled with the cross section for ${}^3\vec{\text{He}}(\vec{e}, e'n)$ and ${}^3\vec{\text{He}}(\vec{e}, e'p)$, respectively. The cross section was taken from calculations [61] because at this low Q^2 it is significantly affected by FSI. A neutron efficiency of $\approx 25\%$ was found in the experiment. With the simulation $\epsilon_n = 21-22\%$ was obtained. For the reasons mentioned above the simulated efficiency is lower and therefore in reasonable agreement.

For the kinematics of this proposal the neutron efficiency was obtained for 6,7 and 8 layers of E-bars for iron absorber thickness between 0 and 4 cm (s. fig. 11). The absorber was placed in between the E-layers. It was not put in front of the first layer because in the offline analysis this layer will be used to check the neutron identification and therefore additional conversion material has to be avoided. It will be considered to use copper plates instead of iron because a magnetic environment could lead to gain shifts of the photomultipliers. From fig. 11 one can see that with increasing absorber thickness the efficiency increases first steeply and at around 2 to 3 cm it saturates slowly. The efficiency indicated by open symbols belong to detector configurations which could also be used in the existing lead box. With the best configuration which consists of 6 E-bar layers with 2 cm iron absorbers one gets $\epsilon_n = 52\%$. An increase of 10 % (relative) would require a new lead shielding.

The misidentification of protons as neutrons was also checked. A conversion factor of around 1.3 % in 2 cm lead was found. Taking into account a neutron detection efficiency of 50 %, the cross section ratio for the reactions ${}^3\vec{\text{He}}(\vec{e}, e'p)$ and ${}^3\vec{\text{He}}(\vec{e}, e'n)$ of 9/4 and a factor 2 for the number of protons in ${}^3\text{He}$ one expects that 6 % of the neutrons were protons before they enter the detector.

3.2.4 Electronics

The electronics for the scintillator will be located on the platform of spectrometer A. A sketch of the coincidence logic is shown in fig. 12. The starting time (common start) is given by the first E-bar which crosses the threshold. It is required that both photomultipliers (PM_{up} and PM_{down}) are above the hardware threshold within a time window of 25 ns. The ADC and TDC information of all channels is read out. The TDC information for the E-bars reaching the threshold later (multiple hits) is recorded relative to the common start. The coincidence between PM_{up} and PM_{down} opens a time window of 100 ns waiting for the trigger from spectrometer A. The time difference between the hadron detector and the spectrometer gives the raw coincidence time. This time is corrected offline for the flight path of the hadron and the electron, the time walk and the position dependent light propagation within the scintillator bar. Applying these corrections a FWHM of 1.8 ns in the coincidence spectrum was achieved which corresponds to a resolution $\sigma = 0.8$ ns. The flight time difference between the fast neutrons of the kinematics in Tab. 1 and particles with velocity close or equal to the one for light (pions, electrons, gammas) is 1.1 ns at a distance of 1.8 m. Even doubling the distance would not result in an unambiguous separation. In view of the solid angle the closer distance is kept. Charged particles



.clip.clip

Figure 12: Sketch of the coincidence logic for the scintillator array/spectrometer A system.

like $\pi^{+/-}$ and electrons are easily identified using the ΔE 's. π^0 's have a short life time of 8×10^{-17} s and they will decay predominantly into two γ 's. Most of the γ 's produce a shower of (charged) particles in the front lead plate and will therefore identified as charged particles. According to the simulation 90 % of γ 's and π^0 's can be removed in this way. This amount could be increased to 95 % when using an upper cut on the ADC's in the E-bars. Their energy deposit shows a much wider distribution than for protons. The remaining fraction will be eliminated with a cut on the invariant mass reconstructed from the measured electron quantities.

3.3 Beam time estimate

The rate r for the reaction ${}^3\text{He}(\vec{e}, e'n)$ measured with the setup shown in Fig. 9 is estimated via

$$r = d\sigma_{en}/d\Omega \Delta\Omega L \epsilon_n \epsilon. \quad (8)$$

The cross section at the central kinematics is 0.14 nb/sr. For the solid angle of spectrometer A the large collimator of 28 msr will be used. The luminosity L is calculated for 5 cm/ $\sin(\theta_e)$ acceptance along the beam line and 5 bar ${}^3\text{He}$ in the target. This results in $L = 3.9$ (nb s) $^{-1}$ for 1 μA . Depending on the configuration of the scintillator array the simulated neutron efficiency ϵ_n ranges from 47 to 57 % for a hardware threshold of 10 MeV (s. sec. 3.2.3). In the following $\epsilon_n = 50$ % is assumed. The factor ϵ takes into account the limited electron momentum acceptance, the momentum distribution of the neutron bound in ${}^3\text{He}$ and radiative corrections which lead to a reduction of the count rate. To estimate their contributions a Monte

Carlo simulation for ${}^3\bar{\text{He}}(\vec{e}, e'n)$ in quasielastic kinematics was performed. This simulation will also serve to support the analysis of the experiment. The kinematics is based on PWIA and uses a momentum distribution fitted to the data of [62]. The radiative tail of the incoming and outgoing electron, energy loss and scattering in materials passed on the way to the detector can be taken into account. The nominal momentum acceptance of $\pm 10\%$ of the central momentum in spectrometer A leads to a reduction of 0.66 in the count rate. Due to the high momentum transfer the Fermi cone is narrow and 91% of the events can be accepted after applying the momentum cut above. This cut removes both wings of the quasielastic bump and therefore reduces also the contribution from high missing momentum p_m . According to the simulation 81% of the events in the acceptance of this experiment have missing momentum of less than 150 MeV/c. The values given above are for the first layer of the neutron detector at a distance of 180 cm. In the subsequent layers a smaller fraction of the Fermi cone will be accepted. This reduction is approximately taken into account due to the reduced solid angle in the overall neutron efficiency.

	efficiency
neutron detector (ϵ_n)	0.5
momentum acceptance	0.66
accepted Fermi cone	0.91
cut on $p_m < 150$ MeV/c	0.8
loss due to radiative tail	0.8

Table 2: Summary of the efficiencies and reduction factors entering eq. 8.

One might be concerned about the events with $p_m > 150$ MeV/c because it is known that FSI and MEC occur particularly at large p_m and that FSI would even shift events to larger p_m . Therefore it would be desirable to have the possibility to cut on $p_m < 150$ MeV/c and for this a reduction of 0.8 is included in ϵ . However, it is clear that p_m cannot be reconstructed from the flight time of the neutron needed to reach the detector because the resolution of the TOF measurement is not sufficient. This would result in a p_m resolution of 600 MeV/c. Using the simulation one finds that a cut on $p_{m\perp} < 150$ MeV/c leaves only 4% of the events with $p_m > 150$ MeV/c. $p_{m\perp}$ is the component of p_m perpendicular to q . Due to the large q $p_{m\perp}$ can be approximately obtained via

$$p_{m\perp} \approx q \tan \theta, \quad (9)$$

where θ is the angle between p' (= momentum of the knocked-out nucleon) and q . It was checked that the result using the equation above is practically undistinguishable from the exact reconstruction. The resolution on $p_{m\perp}$ achieved using eq. 9 is ≈ 23 MeV/c. The value given above takes the resolution of the system into account. The radiative tail of the electrons will smear out the p_m and $p_{m\perp}$ distribution and shift it to larger missing momentum.

The radiative tail will also shift electrons outside the momentum acceptance of spectrometer A. An additional factor of 0.8 accounts for it. A summary of the factors entering eq. 8 via ϵ and ϵ_n is given in Tab. 2.

G_{en} was assumed to be 0.04 which corresponds to the current knowledge of G_{en} (s. fig. 3). With a beam current of 15 μA and aiming at the same statistical error (8.7 %) as E02-013 a data taking period of 300 h is required. During this time the magnetic field direction will be turned approximately every hour passing the target spin directions parallel, perpendicular, antiparallel, antiperpendicular relative to q . These running conditions ensure that sources of systematic errors are kept as small as possible. Because the target cell has to be changed twice a day and Møller measurements have to be performed, an overhead of 30 % is estimated. In addition, beam time for the setup of the neutron detector is needed to check the (modified) data acquisition system, rate studies and optimizing the lead shielding and of the HV. During this test target cells filled with hydrogen and (unpolarized) ^3He as well as empty cells will be used. For this test 30 h are foreseen. The setup of the experiment, installing the polarized ^3He target and the scintillator array with the electronics, is quite elaborate. For this 2 weeks without beam are required. Including the overhead and the tests a beam time of 420 h is requested.

The systematic error consists of the accuracy in G_{mn} (2 %), a possible nuclear correction (3 %) and the accuracy of the measurement with the magnetometer to determine the direction of the magnetic field. The angular uncertainty is estimated to 0.2 % which leads to an error of about 2 % in G_{en} . The direction of the magnetic field will be measured at each of the four magnetic field directions along the target acceptance of the spectrometer. Thus the total systematic error is expected to be 3.5 %.

4 Comparison to E02-013

Experiment E02-013 is scheduled for March 2006 to measure G_{en} at $Q^2 = 1.3, 2.4$ and 3.4 (GeV/c)² with comparable statistical error as proposed here. This experiment will be performed in hall A at Jefferson Lab. An installation time of three month is needed to setup the BigBite spectrometer for the first time, a large scintillator array and the polarized ^3He target with a newly designed magnetic field box. E02-013 has a high figure of merit due to a high pressure target (10 atmospheres) and the large solid angle for electrons (76 msr) with a acceptance of 40 cm target length.

The high performance experiment E02-013 is optimized for high count rates to reach small statistical errors even at the highest Q^2 . In this experiment G_{en} is extracted from the absolute measurement of A_{\perp} . This introduces several systematic errors which drop out in the asymmetry ratio A_{\perp}/A_{\parallel} proposed for the experiment at MAMI. Some of them were already mentioned in sec. 3.1. In addition the magnetic field direction is fixed and can not be aligned with respect to the different directions of \vec{q} for the three Q^2 . A reversal of the magnetic field direction which is usually done to reveal sources of possible "false" asymmetries, is not foreseen.

In the proposal E02-013 the following contributions to the systematic error are considered which will not (or much less) add to the systematic uncertainty of the proposed experiment:

- beam polarization P_e : 3 %
- target polarization P_T : 4 %
- neutron polarization (expected: $0.86 P_T$): 2 %
- dilution factor D (≈ 0.94): 3 %
- dilution factor V (≈ 0.91): 4 %
- correction factor for A_{long} (≈ 0.94): 1 %

The dilution factor D results from 10 times larger admixture of N_2 ($10^{-2}/[{}^3\text{He}]$) which needed for the spin-exchange optical pumping method. V accounts for the unpolarized background. Whereas the online single rates are high because the BigBite gets contributions not only from electrons but also from protons and (positive) pions, this can be reduced offline to ≈ 10 % with a shower counter. Further, experiment E02-013 has to account for a large mixing of A_{\perp} and A_{\parallel} . The measured raw asymmetry is therefore called A_{long} . This is due to the larger acceptance of the BigBite but also due to the use of the same magnetic field direction for all three Q^2 settings. The error given above assumes a field alignment accuracy of 1 mrad (0.06°). Altogether the above contributions add up to 7.4 %.

Further the resolution of A1-spectrometer A is an order of magnitude better, even if one accounts for the reduced resolution due to energy straggling on the 2 mm thick glass of the target cell. This will help to reconstruct the direction of the momentum transfer and to better separate the quasielastic peak from the Δ resonance via the reconstruction of the invariant mass.

In view that E02-013 is the only experiment which is able to measure high $Q^2 > 3$ (GeV/c) 2 using polarized ${}^3\bar{\text{He}}$ the current proposal will serve as an important benchmark for it. Further the region around $Q^2 = 1.5$ (GeV/c) 2 determines the slope of G_{en} and therefore has a large sensitivity to different models. E.g. for the first time a significant deviation from the Galster fit was observed.

A Simultaneous measurement of the magnetic form factor G_{mn} of the neutron

The magnetic form factor of the neutron can be determined from the parallel asymmetry measured in inclusive electron scattering from polarized ${}^3\bar{\text{He}}$. A_{\parallel} is then diluted by the scattering on the two (unpolarized) protons in ${}^3\text{He}$.

$$A_{\parallel} = 2 \frac{\tau \sqrt{1 + \tau + (1 + \tau)^2 \tan^2(\theta/2)} \tan(\theta/2) G_{mn}^2}{(G_{en}^2 + 2G_{ep}^2) + (G_{mn}^2 + 2G_{mp}^2)(\tau + 2\tau(1 + \tau)) \tan(\theta/2)} \quad (10)$$

$$= \frac{a G_{mn}^2}{b + c G_{mn}^2} \quad (11)$$

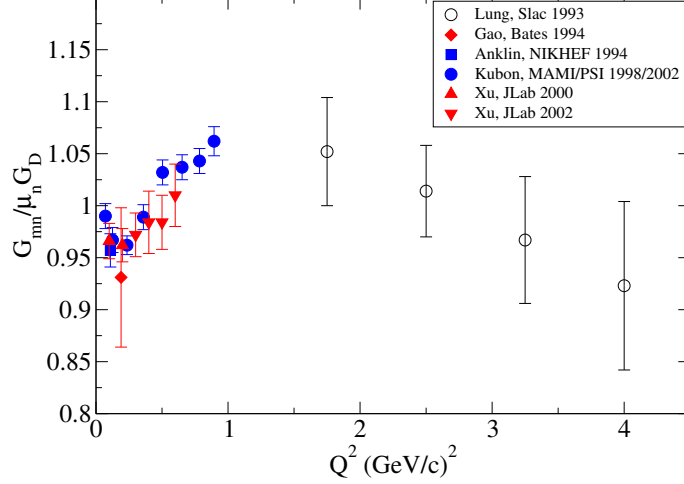


Figure 13: G_{mn} data published since 1990 in units of the dipole form factor as a function of Q^2 . Data in red [63, 64, 65] were measured using polarized ^3He . Data in blue [66, 67, 68] were taken with D exploiting the ratio method.

Contrary to $A_{||}$ in the exclusive reaction $^3\text{He}(\vec{e}, e'n)$ (s. eq. 5) G_{mn} does not drop out in eq. 10. For the low to medium Q^2 range the first term b in the denominator is much larger the one containing G_{mn}^2 (factor five at our kinematics). This method was already exploited in three experiments at Bates and in Hall A [63, 64, 65]. Their results are shown in fig. 13. It was argued that at the higher Q^2 values no correction accounting for the ^3He structure and reaction mechanisms is necessary. The data of [69] were taken in inclusive e-D scattering in quasielastic kinematics. This has the disadvantage that the large proton part has to be subtracted. In addition this method requires a separation of the cross section in transversal and longitudinal response even at high Q^2 . The most precise data shown in fig. 13 have measured the cross section ratio $R = D(e,e'n)/D(e,e'p)$. This minimizes the dependence on the deuteron model because the ratio is independent of the deuteron wave function as the momentum distributions are identical for proton and neutron. The drawback is that this method requires the knowledge of the neutron detection efficiency. The same method was used to measure G_{mn} with CLAS at Jlab. In a broad Q^2 range from 0.6 to 4 $(\text{GeV}/c)^2$ a small uncertainty of 2 - 3 % will be achieved. Preliminary results are published in [44].

Simultaneously to the G_{en} measurement inclusive $^3\text{He}(e,e')$ data can be taken with spectrometer A. The expected statistical error is 6.8 % assuming the dipole value for G_{mn} . With a similar uncertainty as the actual high Q^2 values of ref. [69] this measurement clearly cannot compete with the measurement done at CLAS. However, it will serve as a check for our G_{en} measurement. In addition to the statistical error there will be a systematic uncertainty mainly from the absolute determination of the target and electron polarization.

References

- [1] J.D. Ashley, D.B. Leinweber, A.W. Thomas, and R.D. Young, Eur. Phys. J. A **19** s01, 9 (2004)
- [2] M. Guidal, M. V. Polyakov, A. V. Radyushkin, and M. Vanderhaeghen, arXiv:hep-ph/0410251
- [3] E.L. Lomon, Phys. Rev. **C66**, 045501 (2002)
- [4] H.-W. Hammer and Ulf-G. Meißner, Eur. Phys. J. **A 20**, 469 (2004)
- [5] M. K. Jones *et al.*, Phys. Rev. Lett. **84**, 1398 (2000)
- [6] O. Gayou *et al.*, Phys. Rev. Lett. **88**, 092301 (2002)
- [7] K. Kawarabayashi and M. Suzuki, Phys. Rev. Lett. **16**, 255 (1966), Riazuddin and Fayyazuddin, Phys. Rev. **147**, 1071 (1966)
- [8] G. Holzwarth, arXiv:hep-ph/0201138, Z. Phys. **A356**, 339 (1996)
- [9] G.A. Miller, Phys. Rev. **C66**, 032201(R) (2002)
- [10] J. Friedrich and Th. Walcher, Eur. Phys. J. A **17**, 607 (2003)
- [11] H.-W. Hammer, D. Drechsel, Ulf-G. Meißner, Phys. Lett. **B 586**, 291 (2004)
- [12] S. Kopecky *et al.*, Phys. Rev. Lett. **74**, 2427 (1995)
- [13] S. Kopecky *et al.*, Phys. Rev. **C56**, 2229 (1997)
- [14] N. Isgur, Phys. Rev. Lett. **83**, 272 (1999)
- [15] A.J. Buchmann, Phys. Rev. Lett. **93**, 212301 (2004)
- [16] I. Passchier *et al.*, Phys. Rev. Lett. **82**, 4988 (1999)
- [17] C. Herberg *et al.*, Eur. Phys. J **A5**, 131 (1999)
- [18] M. Ostrick *et al.*, Phys. Rev. Lett. **83**, 276 (1999)
- [19] J. Becker *et al.*, Eur. Phys. J. **A6**, 329 (1999)
- [20] H. Zhu *et al.*, Phys. Rev. Lett. **87**, 081801 (2001)
- [21] J. Bermuth *et al.*, Phys. Lett. **B564**, 199 (2003)
- [22] R. Madey *et al.*, Phys. Rev. Lett. **91**, 122002 (2003)
- [23] G. Warren *et al.*, Phys. Rev. Lett. **92**, 042301 (2004)
- [24] D.I. Glazier *et al.*, Eur.Phys.J. **A24**, 101 (2005)
- [25] R. Schiavilla and I. Sick, Phys. Rev. **C64**, 041002(R) (2001)

- [26] I.A. Quattan *et al.*, Phys.Rev.Lett. **94**, 142301 (2005)
- [27] P.A.M. Guichon and M. Vanderhaeghen, Phys. Rev. Lett. **91**, 142303 (2003)
- [28] P.G. Blunden, W. Melnitchouk, and J.A. Tjon, Phys. Rev. Lett. **91**, 142304 (2003)
- [29] S. Galster *et al.*, Nucl. Phys. **B32**, 221 (1971)
- [30] S. Platchkov *et al.*, Nucl. Phys. **A510**, 740 (1990)
- [31] M.M. Kaskulov and P. Grabmayr, Eur. Phys. J. **A19**, 157 (2004)
- [32] C.J. Bebek *et al.*, Phys. Rev. **17**, 1693 (1978)
- [33] J. Volmer *et al.*, Phys. Rev. Lett. **86**, 1713 (2001)
- [34] S.R. Amendolia *et al.*, Nucl. Phys. B **277**, 168 (1986)
- [35] R.G. Arnold, C.E. Carlson, F. Gross, Phys. Rev. **C23**, 363 (1981)
- [36] B. Anderson, J. Kelly, S. Kowalski, R. Madey, A. Semenov (spokespersons), proposal PR-04-110, Jefferson Lab, 2004
- [37] M. Distler, W. Heil, D. Rohe (spokespersons), A1/2-00 proposal at MAMI, 2000
- [38] P. Achenbacher *et al.*, accepted by Eur. Phys. J. A
- [39] D. Rohe *et al.*, Phys. Rev. Lett. **83**, 4257 (1999)
- [40] R.G. Milner *et al.*, Phys. Lett. B **379**, 67 (1996)
- [41] R.W. Schulze and P.U. Sauer, Phys. Rev. **C48**, 38 (1993)
- [42] D. Rohe, PhD thesis at the University of Mainz, 1998
- [43] W. Brooks (contact person), proposal E94-017, Jefferson Lab, 1994
- [44] W. K. Brooks, J. D. Lachniet *et al.*, Nucl. Phys. A **755** 261
- [45] J. Golak *et al.*, Phys.Rev. **C66**, 024008 (2002)
- [46] H.R. Poolman, PhD thesis at the University of Amsterdam, 1999
- [47] M. Sargsian, Int.J.Mod.Phys. **E10**, 405 (2001)
- [48] J. Golak *et al.*, Phys. Rev. **C65**, 064004 (2002)
- [49] A. Deltuva, Phys. Rev. **C70**, 034004 (2004)
- [50] C. Carasco *et al.*, Phys. Lett. **B 599**, 41 (2003)
- [51] M. Meyerhoff *et al.*, Phys. Lett. B **327**, 201 (1994)

- [52] J.M. Laget, Phys. Lett. B **273**, 367 (1991)
- [53] J.M. Laget, Phys. Lett. B **276**, 398 (1992)
- [54] H. Kamada, W. Glöckle, J. Golak, Ch. Elster, Phys. Rev. **C66**, 044010 (2002)
- [55] P. Bartsch, PhD thesis at the University of Mainz, 2001
- [56] E.W. Otten, Europhysics News **35**, 16 (2004)
- [57] N.R. Newbury *et al.*, Phys. Rev. **A48**, 4411 (1993)
- [58] T.E. Chupp *et al.*, Phys. Rev. **C45**, 915 (1992)
- [59] S. Baeßler, private communication
- [60] S. Agostinelli *et al.*, Nucl. Instr. & Meth. **A 506** 250 (2003)
- [61] J. Golak, private communication
- [62] R.E.J. Florizone *et al.*, Phys. Rev. Lett. **83**, 2308 (1999)
- [63] H. Gao *et al.*, Phys. Rev. **C50**, 546R (1994)
- [64] W. Xu *et al.*, Phys. Rev. Lett. **85**, 2900 (2000)
- [65] W. Xu *et al.*, Phys. Rev. **C67**, 012201R (2002)
- [66] H. Anklin *et al.*, Phys. Lett. **B336**, 313 (1994)
- [67] H. Anklin *et al.*, Phys. Lett. **B428**, 248 (1998)
- [68] G. Kubon *et al.*, Phys. Lett. **B524**, 26 (2002)
- [69] A. Lung *et al.*, Phys. Rev. Lett. **70**, 718 (1993)